A Novel Assistive Imaging Device for Colon Map Reconstruction

Neri Niccolò Dei, Sophia Bano, *Member, IEEE*, Francisco Vasconcelos, Vanni Consumi, *Student Member, IEEE*, Danail Stoyanov, *Fellow, IEEE*, Agostino Stilli, *Member, IEEE*, and Gastone Ciuti, *Senior Member, IEEE*

***Abstract*—Colonoscopy, recognised as the gold standard for diagnosing and treating colorectal cancer, faces limitations that may result in overlooking some colonic regions. This can lead to missed lesions and interval cancer, leading to incomplete treatment. Addressing this challenge, the authors present a novel Assistive Imaging Device for Colon Map Reconstruction (AID-CMR) to support clinicians in visualising the entire colonic mucosa and identifying areas that may have been missed during the procedure. The device is comprised of an overtube tooled with an imaging module on its distal end, which can be moved about a threaded silicone sleeve. The imaging module houses inflatable silicone chambers to distend the lumen, a side-viewing miniaturised full-HD camera with LEDs, a magnetic encoder, and an irrigation channel for camera cleansing. Before intervention, the device can be installed on standard colonoscopes or other tethered endoscopes. During the intervention, the device can be operated to (1) reconstruct assistive maps of the organ, (2) visualise the full anatomy, and (3) increase disease detection. Moreover, these maps may be employed for the quantification of missed regions during standard inspection. This letter introduces a proof of concept device and discusses locomotion and reconstruction tests conducted in two in-vitro conditions. These tests reveal overall procedural feasibility in terms of locomotion, exerted forces and colon map reconstruction, preserving polyp morphology.**

***Index Terms*—Medical robots and systems, soft robot materials and design, computer vision for medical robotics, colon reconstruction, robotic-assisted colonoscopy.**

I. Introduction

COLONOSCOPY is the gold standard for the detection and treatment of colorectal cancer (CRC), the second most common cause of cancer-related death worldwide [1]. Although colonoscopy screening programs have been shown to reduce the incidence and mortality of CRC, the practice is imperfect, and many improvements can be made to reduce the miss-rate of adenomas [2], which may be as high as 33% for individuals at risk of CRC [3]. Among the risk factors associated with CRC miss-rate, incomplete bowel inspection, mainly due to insufficient bowel preparation and endoscopist technique and expertise, is of paramount importance [4]. Improving colonoscopy performance is vital to mitigate the threat of CRC and its associated costs. Colonoscopy performance is assessed through multiple quality indicators, among which the adenoma detection rate (ADR) is the most relevant as it is directly associated with the morbidity and mortality of interval CRC [5]. This parameter measures the rate of precancerous lesions that are identified and removed during a colonoscopy procedure.

Currently, endoscopists lack reliable tools to quantify the percentage of inspected mucosa during colonoscopy. Moreover, the identification of polyps requires thorough manual scope retrospection, posing potential risks of clinician fatigue and injury [2]. To address these challenges, new hardware and software systems have been proposed in recent years [2]. On the software side, the reconstruction of the colon from the endoscope's front-facing camera is still an unsolved task, as exemplified by the recent MICCAI 2022 Endoscopic Vision

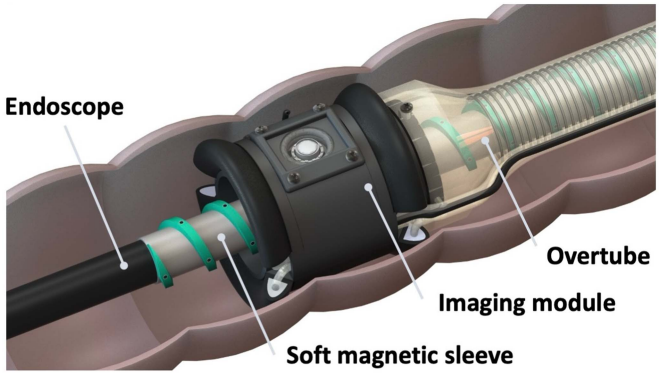

Fig. 1. Digital rendering illustrating the components of AID-CMR. An overtube, coaxial with the endoscope, carries an imaging module at its tip which houses a side-viewing camera. The system is moved manually through external rotation of the overtube. The imaging module travels about a helical path provided by the soft magnetic sleeve, which is fixed to the endoscope and extends 252 mm from just before the articulated tip of the endoscope.

Received 6 May 2024; accepted 29 September 2024. Date of publication 14 October 2024; date of current version 21 October 2024. This article was recommended for publication by Associate Editor N. Gravish and Editor Y.-L. Park upon evaluation of the reviewers' comments. This work was supported in part by the Wellcome/EPSRC Centre for Interventional and Surgical Sciences (WEISS) under Grant 203145/Z/16/Z, in part by the Department of Science, Innovation and Technology (DSIT), and in part by the Royal Academy of Engineering Chair in Emerging Technologies Scheme under Grant CiET1819/2/36. *(Corresponding author: Neri Niccolò Dei.)*

Neri Niccolò Dei and Gastone Ciuti are with the BioRobotics Institute and Department of Excellence in Robotics and AI, Scuola Superiore Sant'Anna, 56127 Pisa, Italy (e-mail: neriniccolo.dei@santannapisa.it; gastone.ciuti@santannapisa.it).

Sophia Bano, Francisco Vasconcelos, Vanni Consumi, Danail Stoyanov, and Agostino Stilli are with the Hawkes Institute and Department of Computer Science, University College London, W1W 7TY London, U.K. (e-mail: sophia.bano@ucl.ac.uk; f.vasconcelos@ucl.ac.uk; vanni.consumi.20@ucl.ac.uk; danail.stoyanov@ucl.ac.uk; a.stilli@ucl.ac.uk).

This letter has supplementary downloadable material available at https://doi.org/10.1109/LRA.2024.3479704, provided by the authors.

Digital Object Identifier 10.1109/LRA.2024.3479704

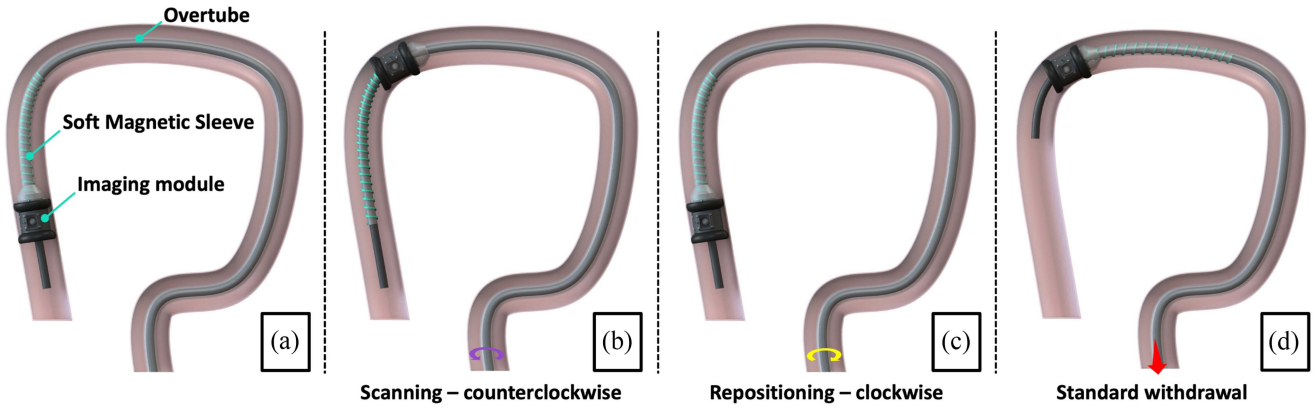

Fig. 2. Digital rendering illustrating the four operative phases of AID-CMR. (a) *Starting phase:* the imaging module is located at the distal end of the SMS. (b) *Scanning phase:* the overtube is rotated counterclockwise (purple arrow) to withdraw the imaging module until the proximal end of the SMS. During withdrawal, the device moves about the helical thread of the SMS while reconstructing the assistive map. (c) *Repositioning phase:* the overtube is rotated clockwise (yellow arrow) to position the imaging module back to the starting position. (d) *Withdrawal phase:* the endoscope, along with the device, is withdrawn (red arrow) as per standard colonoscopy practice, leveraging the assistive map generated in (b) to find lesions. Once the endoscope is withdrawn by an amount equal to the length of the SMS, a new starting position can be defined, and the imaging process can start over.

Challenge "SimCol-to-3D 2022 - 3D Reconstruction During Colonoscopy" [6]. This challenge dealt with the estimation of depth maps and endoscope poses for the reconstruction of the organ using state-of-the-art computer vision techniques. While larger and more comprehensive datasets are increasingly being published and shared within the research community [7], [8], a significant challenge to these methods is the absence of in-vivo datasets; a major limitation for clinical translation.

On the hardware side, to the best of our knowledge, there are no devices specifically designed for the reconstruction of assistive maps of the colon. Devices such as large field-of-view (FoV) endoscopes have been developed, e.g., the Full Spectrum Endoscopy (FUSE, EndoChoice), which offers a standard forward-viewing camera and two additional left and right lateral cameras. A multicentre perspective randomised trial of tandem colonoscopy comparing the third generation of FUSE to standard forward-viewing colonoscopy concluded that the system did demonstrate statistically significant difference in adenoma miss-rate [9]. Some of its limitations include its inferior maneuverability [9]. The Third-Eye Panoramic cap (Avantis Medical Systems, USA) is an add-on colonoscopy device equipped with two side-facing cameras. It can be installed on the distal end of the endoscope prior to intervention. These cameras collect three distinct images, which are presented on a screen, thereby expanding the visual field to beyond 300° [10]. This device has been exclusively tested in a feasibility study, which assessed its impact on achieving cecal intubation. The findings of the study indicate that this supplementary tool unveiled polyps and diverticula that were initially overlooked when using the standard front-facing endoscope alone [10]. Lastly, a colonoscopy add-on consisting of a distal cap equipped with two side-viewing cameras, along with artificial intelligence (AI) algorithms for polyp detection, has recently been presented in [11], showing promising results in adenoma detection in porcine in-vivo tests.

The exploration of side-viewing hardware solutions holds promise for innovative concepts in colonoscopy, potentially enhancing detection and diagnosis through additional image views and direct imaging of the colon wall. Building on this research trajectory, a novel Assistive Imaging Device for Colon Map Reconstruction (AID-CMR) has been designed and developed. The device, illustrated in Fig. 1, consists of three components: an overtube, an imaging module, and a soft magnetic sleeve (SMS). This article introduces a proof of concept of AID-CMR. Its components are detailed in Section II. Experimental tests including a locomotion test within a colon simulator, and a map reconstruction test within a textured colon simulator are discussed in Section III. Section IV discusses current limitations and next steps.

II. Materials and Methods

A proof of concept of AID-CMR is illustrated in Fig. 1. Starting from a 1.7:1 scale system (currently measuring 39 mm in diameter at the imaging module, and a miniaturised target of 23 mm), a preliminary working prototype comprised of the three listed components has been designed. These are functional proof of concepts that will be further miniaturised and optimised in future developments. The overtube serves as the means of locomotion of the imaging module, which is installed at its tip. The imaging module houses a side-viewing full-HD camera and is moved about a helical path provided by the SMS, fixed on the endoscope, which guarantees a precise trajectory of the camera and a proxy for robust camera pose estimation.

A. Working Principle

Before the intervention, the device is installed on a compatible standard colonoscope or other tethered endoscopes, before the articulated distal portion of the scope. The current proof of concept is based on a 13803 PKS endoscope (Karl Storz SE & Co. KG, Germany) with an outer diameter of 11.3 mm. During cecal intubation, the inflatable chambers on the imaging module are slightly inflated, working as soft bumpers to protect the mucosa from the rigid chassis, as illustrated in Fig. 1. The working principle of AID-CMR is illustrated in Fig. 2. Once the cecum has been reached, prior to standard endoscope withdrawal, the assistive map reconstruction can be initiated by the endoscopist

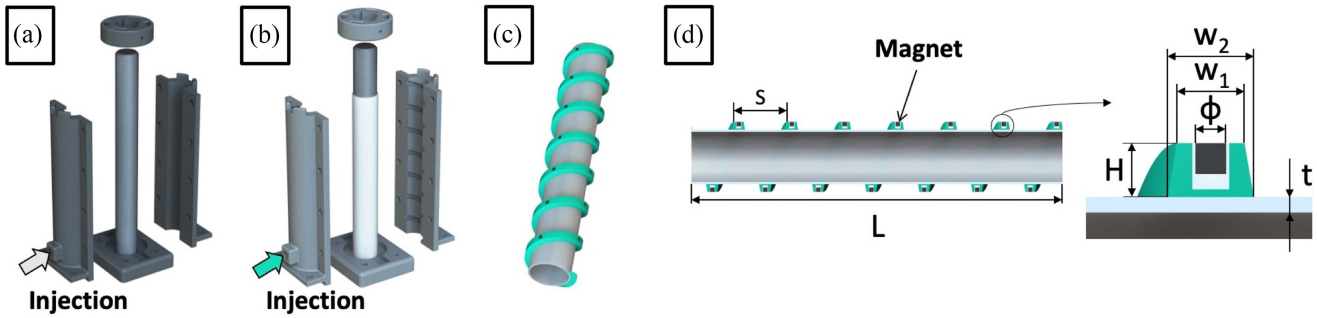

Fig. 3. The soft magnetic sleeve design and manufacturing. (a) The SMS is manufactured in modules of length L = 84 mm via silicone injection molding. A soft silicone core is realised first. (b) A hard silicone thread is over-moulded on top of the core. (c) Cylindrical N45 magnets with a 1 mm height and diameter are glued inside dedicated cavities along the thread, located every 90°. (d) Section and detailed views of the SMS. The step size of the thread is $S = 12$ mm. The thickness of the core is $t = 0.5$ mm. The thread profile is a trapezoid with height $H = 1.75$ mm, lower base $W2 = 2.8$ mm and upper base $W1 = 2.2$ mm.

(*Starting phase*, Fig. 2(a)). The map reconstruction is started at the control station (a computer) and generated while externally rotating the overtube counterclockwise to withdraw the imaging module (*Scanning phase*, Fig. 2(b)). The map is updated in real-time and available for immediate consultation at the control station.

The colon is a challenging organ to inspect because of its deformable and dynamic nature (e.g., elastic tissue, peristalsis, and segmentation). To target this issue, the imaging module is tooled with pneumatic silicone chambers installed on both sides of the camera. These can be inflated and deflated to adjust the spreading of the colonic mucosa to improve visualisation. A pneumatic control interface is available at the control station for controlling and monitoring the internal pressure, as detailed in Section II.C. Once withdrawn until the proximal end of the SMS, the handle of the overtube is designed to meet the handle of the endoscope, and used as mechanical stop. The endoscopist rotates the imaging module back to the starting position, by turning the overtube clockwise (*Repositioning phase*, Fig. 2(c)). The generated map can be consulted by the endoscopist to estimate the presence of lesions or other signs of pathology along the inspected colon tract. The endoscope can be withdrawn following the standard procedural practice, e.g., to reach the areas of interest identified in the generated assistive map (*Withdrawal phase*, Fig. 2(d)). A subsequent assistive map can be generated at a new starting position (e.g., at the end of the previous one, estimated by checking the graduated scale on the endoscope). The procedure can be performed iteratively until complete withdrawal. This iterative solution has been conceived for two reasons: first, the overtube can only be withdrawn up to a certain length before reaching the handle of the endoscope. Secondly, such segmentation allows analysing one anatomical region after the other, as the screening procedure progresses. This allows to concentrate on smaller, more manageable assistive maps. Moreover, studies have shown that different types of lesions have variable prevalence across the colon anatomical segments [12]. The following section illustrates each component in detail.

B. System Components

The three system components, illustrated in Fig. 1, are detailed below. The overtube is the locomotion means for the imaging module, which is installed at its tip, and is manually moved by the endoscopist. The imaging module houses the side-viewing camera to image the colonic mucosa. It is moved about the SMS, which is made of silicone materials and houses cylindrical magnets sensed by the magnetic encoder.

1) Overtube: The overtube has been obtained by re-purposing a colonoscopy medical device. The discontinued Entrada overtube (US Endoscopy, USA), designed as an add-on device for sigmoid straightening during colonoscopy, was chosen as overtube due to its flexibility and torsional stiffness. The overtube is composed of a metallic spring reinforcement within a polymeric matrix, which effectively transmits torque from the handle to the tip while maintaining a high flexibility, limiting the impact on the maneuverability of the endoscope. The overtube is compatible with scopes whose outer diameter is in the range 11.1–13.7 mm. It has an operative length of 40 cm, and internal and external diameters of 16.9 and 19.8 mm, respectively. For our application, the overtube was modified, removing its handle and using the remaining polymeric joint as a link to connect to the imaging module. During our initial tests utilizing the mentioned endoscope with an operative length of 110 cm, it was determined that the maximum practical length for the overtube is 80 cm. Therefore, two Entrada overtubes have been connected in series to obtain an 80 cm long one. In the future, an ad-hoc overtube will be developed, considering industrial manufacturing processes and multi-material 3D printing for its realisation.

2) Soft Magnetic Sleeve: The soft magnetic sleeve (SMS) is the mechanical guide of the imaging module. Its manufacturing process, dimensions, and assembly are illustrated in Fig. 3.

The SMS consists of a soft silicone core and an over-moulded hard silicone thread. The silicone core is manufactured via injection moulding using a combination of 3D printed resin moulds and an aluminum core, as illustrated in Fig. 3(a). The core material is Dragon Skin 20 (Smooth-On Inc., USA), and its thickness measures 0.5 mm. The inner diameter corresponds to the outer diameter of the employed endoscope. This silicone was chosen empirically for its durability while considering to keep the added scope rigidity and radial bulk to a minimum. After curing, the aluminium core and silicone cylinder are moved to the thread mould (Fig. 3(b)). Here, Smooth-Sil 960 (Smooth-On Inc., USA) is injected to realise the thread. This harder silicone is used to limit wear during operation.

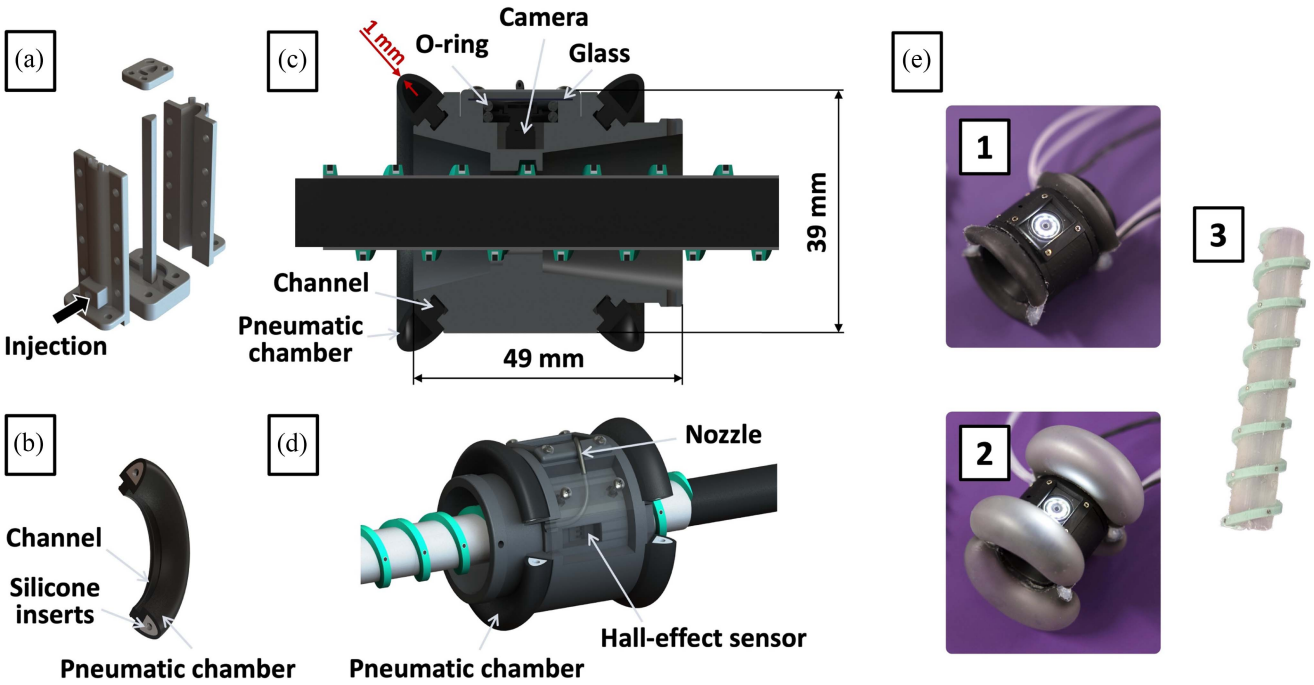

Fig. 4. Design details of the imaging module. (a) The pneumatic chambers on the imaging module are manufactured via silicone injection moulding. Straight chambers are realised, and then curved onto the device during installation. (b) The extremities of each chamber are fitted with silicone inserts with cylindrical holes for connecting pneumatic lines. (c) Section view of the imaging module illustrating the threaded connection with the SMS mounted on the endoscope. A protective glass is placed on top of the camera and pressed on two o-rings by a camera lid. The chassis measures 39 mm in outer diameter and 49 mm in length. (d) The Hall-effect sensor is placed on one side of the device, facing radially towards the SMS' magnets. Details such as cables are not illustrated for clarity. (e) Photographs of the realised components. The imaging module is displayed with deflated (1) and inflated (2) chambers next to an SMS (3).

Within the threaded mould cavity, cylindrical extrusions with a diameter and height of 1.2 mm are positioned at the center of the thread, spaced 90° apart. These structures serve to create hollow cavities within the silicone thread, intended for accommodating cylindrical N45 magnets with dimensions of 1 mm in diameter and height. These magnets are employed to realise a magnetic encoder, as detailed in the imaging module subsection. The SMS is manufactured in 84 mm long modules, with seven thread revolutions spaced 12 mm apart. A working length of 252 mm is obtained by gluing together three units to obtain a full-length SMS. In the future, the SMS will be directly manufactured in its full length using a machined set of moulds. The thread pitch has been chosen to allow large image overlap between frames one revolution apart. The thread profile is trapezoidal and was designed with minimal radial bulk while providing a stable path with low friction. Initially considering a square thread profile for the imaging module due to its theoretical advantages in minimising friction, we opted for a trapezoidal shape in light of manufacturing practicality. Fabrication challenges and potential silicone deformation during contact with the rigid thread on the imaging module led to the current design, illustrated in Fig. 3(d), which resulted from empirical comparisons of various dimensions and aspect ratios. The thread profile will be optimised in future developments using a parametric search.

3) Imaging Module: The imaging module is the distal component of AID-CMR, and houses a side-viewing full-HD camera to image the colon walls. The camera (MISUMI Electronics Corp., Taiwan) has a FoV of 158° and hosts ten controllable high-intensity LEDs. The lens focuses at 15 mm, although a clear picture is achieved in the range 8–35 mm. The focus distance is approximately at the average colon diameter in prone and supine positions [13] (i.e., 41 mm, or 69.7 mm when scaled by the prototype scale factor). The focus range adequately covers the colon, capturing sharp visuals from its narrowest to widest sections. Indeed, the internal diameter of the colon spans on average from a minimum of 26 mm at the sigmoid to a maximum of 45 mm at the ascending colon [13]. Scaling these values by the prototype scale factor, the imaging module can image both regions sharply. Specifically, the average sigmoid can be imaged clearly after dilating the pneumatic chambers by approximately 2 mm along the radial direction. The camera can also image the widest colon region clearly because it falls within the focus range.

The chassis of the imaging module comprises four components: a main body, two lateral lids (on opposite sides, one to cover the Hall-effect sensor and one to cover the pneumatic and camera lines), and a camera lid. The main component is threaded with the same thread profile used for the SMS, enlarged to have a play of 0.2 mm on all sides. All components are installed onto the main one through M1.6 screws and nuts. The latter are embedded into dedicated cavities within the main part. As illustrated in Fig. 4(c), the camera is mounted on the main component and secured in place with silicone glue. Two o-rings encircle the lens, protecting against dust and water. These are compressed firmly by a protective glass, held in position by the camera lid. Internally, the main part of the chassis features a conical cut, aiding in maneuverability during curves.

The colon tissue can be spread by actuating four pneumatic chambers illustrated in Fig. 4(c), 4(d) and 4(e). These have a semi-elliptical cross-section with a 1 mm thickness, and are installed in pairs on the two sides of the camera at a 45° angle. The angle limits camera field of view hindering during inflation. The chambers can be inflated up to a limit pressure equal to 10 kPa, well within the actuation limit of 200 kPa suggested in [14]. This pressure range can expand a chamber radially to circa 16.5 mm, which allows spreading even the largest colonic segment (i.e., the ascending colon) in the scaled colon case. Similarly, these chambers can dilate the average human colon, in case they were to be employed on a 1:1 scale device. The chambers are manufactured via injection moulding using EcoFlex 00-50 silicone adding SLIDE^{TM} STD Liquid Surface Tension Diffuser (both by Smooth-On Inc., USA) to reduce its friction, as illustrated in Fig. 4(a). The silicone material was selected empirically, comparing the performance of different silicones in terms of flexibility and radial expansion. The silicone is pigmented in black to maximise the absorption of light reflections on the shiny mucosa. On the chassis, curved grooves angled at 45° with respect to the horizontal axis are designed to host the channel running along the bottom of each chamber. This channel has a cross-section larger than the one on the chassis groove, realising a snap elastic fit (Fig. 4(c)) which is further reinforced with silicone glue (Sil-Poxy, Smooth-On Inc., USA). Two silicone inserts are glued on both ends of the chamber to allow the insertion of pneumatic lines (Fig. 4(b)). The inserts are manufactured using Dragon Skin 30 (Smooth-On Inc., USA), as the stiffness of this material closely matches the one of the glue used for their installation. Inserts are manufactured by depositing silicone on semi-elliptical cavities obtained by laser-cutting a 3 mm thick polymethyl methacrylate (PMMA) sheet. Each of these cavities hosts a central aluminium rod, realising a 2 mm cylindrical hole to fit a pneumatic line. Once glued to the chamber, the distal insert is sealed with glue, while the proximal one is fitted with a 2 mm pneumatic silicone tube. Each pair of chambers is inflated using a shared pneumatic line, and symmetrical expansion is achieved. As illustrated in Fig. 4(d), one side of the imaging module hosts a Hall-effect sensor (Honeywell SS496A1) to realise a magnetic encoder when moving on the SMS. A simulation of the magnetic field intensity of the SMS magnets was computed using MATLAB (The MathWorks Inc., USA) libraries. The selected sensor is analog and its output signal is a voltage whose value changes when a magnetic field is sensed. Signal processing and a delay time between two magnetic field readings allow the system to be robust to misreadings and repeated readings of the same magnet. The magnetic encoder does not allow identifying the exact location of the imaging module along the SMS, nor in which direction it is rotating. However, given a fixed locomotion direction, it is useful for estimating the relative pose of the camera along the colon for the computer vision pipeline, as detailed in Section III. Using two half chambers instead of a single one simplifies the manufacturing process and allows the camera, Hall-effect sensor, hydraulic, and pneumatic lines to pass along the sides of the chambers (Fig. 1), reducing the total encumbrance. Accordingly, the outer diameter of the imaging module chassis is 39 mm, and corresponds to the total outer diameter when the pneumatic chambers are vacuumed. This will be further miniaturised, targeting an outer diameter of 23 mm towards clinical implementation, as described in Section IV. Photographs of the realised components are displayed in Fig. 4(e). An assembled imaging module is portrayed in deflated and inflated states, next to an assembled SMS.

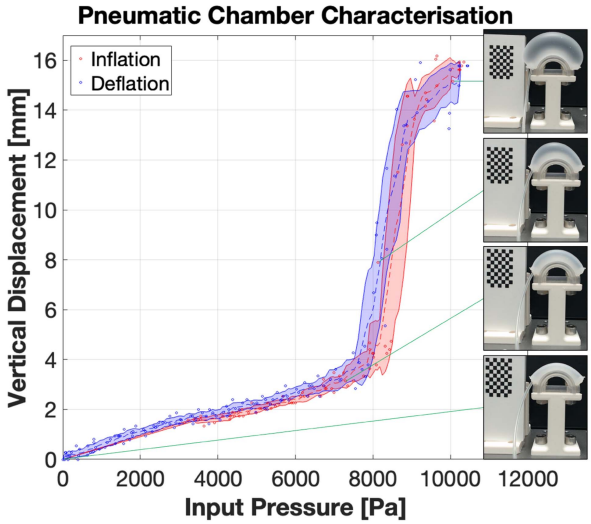

Fig. 5. Pneumatic chambers characterisation. The graph depicts the relationship between input pressure (Pa) and vertical displacement (mm) of the chamber. The red and blue points illustrate data from five inflation and deflation experiments, respectively. Dashed curves represent the average trend calculated through a moving average filter with a 10-sample window, while shaded areas indicate the associated confidence intervals. On the right, four illustrative examples present the shape of the pneumatic chamber at different input pressures. The pneumatic chamber is fixed to a 3D-printed support and a checkerboard is used as reference for calibrating the image-based characterisation pipeline.

C. Pneumatic Chambers Characterisation

The inflatable chambers have been characterised to determine the relationship between input pressure and outer diameter. As illustrated in Fig. 5, a pneumatic chamber has been installed on a fixed 3D printed support, connected to a pneumatic line, and imaged with a fixed full-HD webcam. Using an image-based approach, as presented in [15], the expansion of the chamber is determined by manually selecting the upper vertical point within a MATLAB (The MathWorks Inc., USA) script. To determine the relationship between pixels and millimeters, a checkerboard is used for calibration. The chamber is inflated using a pressure regulator (VPPX-6F-L-1-F-0L10H-S1, FESTO GmbH, Germany), connected to a DAC (DA4C010BI, APTINEX Ltd., Sri Lanka). The system is voltage-controlled and pressure inputs are regulated in steps using a gamepad connected to an STM32 Nucleo-64 microcontroller (STMicroelectronics N.V., Switzerland). The input pressure is monitored continuously through the manometer within the pressure regulator. A picture of the chamber is saved along with the corresponding pressure, obtained mediating registered values during a three-second window, one minute after each input step to allow material relaxation and to reach a steady state. Five experimental tests, each for inflation and deflation, have been conducted. The resulting relationship

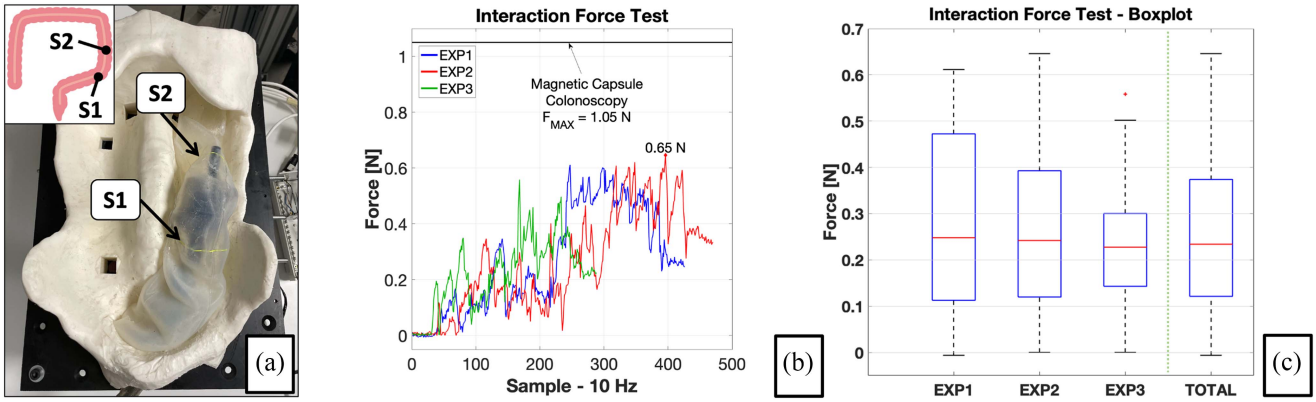

Fig. 6. Locomotion experiment. (a) The experimental setup features the colon simulator within an abdominal phantom, as employed in [16], [17]. Two mono-axial force sensors are connected to the colon via inextensible cables and positioned on the lower (S1) and upper sigmoid (S2). (b) The graph illustrates the results from three withdrawal tests. The measured forces are recorded at the sampling frequency of 10 Hz and the highest value between the two sensors is plotted. Experiment 2 recorded the maximum force, reaching 0.65 N. The black line at the top indicates the maximum force registered by magnetic capsule colonoscopy in a similar *ex-vivo* test [16]. (d) Boxplot for each experimental test and for the whole set of experimental data. The median is reported in red, along with the 25th and 75th percentiles, within the blue box. An outlier in experiment three is highlighted with a red cross.

is illustrated in Fig. 5. The blue and red points represent the recorded pressure values and corresponding vertical displacement during inflation and deflation tests, respectively. For both, a moving average with a window of ten data points has been calculated and plotted using a spline curve, and an error band corresponding to the confidence interval is illustrated around each. The chamber expansion is almost linear up until 8000 Pa circa. Then, the silicone material expands more abruptly, bulging upwards. The trend then meets a plateau around 9000 Pa. Inflation is stopped at 10 kPa, corresponding to the displacement necessary to dilate the largest colon section.

III. Experimental Setup and Results

Two main experiments have been carried out to demonstrate the functionality of the prototype. A curved in-vitro colon simulator has been employed to demonstrate the locomotion performance and evaluate forces exerted by the device on the colon walls. To demonstrate the assistive map generation, a 2D mosaicking panoramic reconstruction test has been performed in another in-vitro colon simulator with textured vessel structures.

A. Locomotion Test

The colon simulator for the locomotion test has been manufactured using modular moulds presented in [17]. Three segments manufactured with EcoFlex 00-31 Near Clear (Smooth-On Inc., USA), one curved 90° and two straight, were connected together to replicate a curved colon. Although the authors in [17] used a harder silicone (EcoFlex 00-50) as the optimal trade-off between ease of manufacturing and realistic mechanical properties, our material choice has been made to compensate for the increment in stiffness due to the larger, scaled thickness of the colon segments, by using a softer silicone. As for the pneumatic chambers, the silicone colon phantom has been manufactured with SLIDE^{TM} STD Liquid Surface Tension Diffuser (Smooth-On Inc., USA) to reduce friction. This simulator replicates a sigmoid colon tract, scaled with the 1.7:1 scale factor used for the whole prototype. In humans, the sigmoid is the narrowest colon region [13]. Therefore, this represents the worst-case scenario in which the prototype has to move through the narrowest anatomical segment, with highest friction. The locomotion tests have been performed by a single person with no clinical background, installing the device on the selected endoscope and inflating its chambers with a pressure of 8000 Pa (enough to dilate the sigmoid phantom to a distance at which the camera can focus). After lubricating the colon phantom with a water-based endoscopy lubricant, it has been placed within a sensorised anatomical model of the human abdomen (OVESCO Endoscopy AG, Germany), as conducted in [16], [17], over the upper and lower sigmoid. As depicted in Fig. 6(a), two mono-axial force sensors have been placed around the lower and upper sigmoid and connected through inextensible cables stitched to the phantom. Three withdrawal experimental tests have been conducted, measuring a peak force of 0.65 N (Fig. 6(b)). This is just a third of the maximum force exerted by the standard endoscope and, for reference, about 60% of the force exerted by magnetic capsule colonoscopy, as reported in [16] for the same anatomical region using the same abdominal phantom. During insertion, the uninflated device is smaller than any colon section, and insertion forces have been evaluated through repeated experiments, measuring largely smaller force peaks than those measured during withdrawal. Hence, solely withdrawal tests are reported, during which the inflation of the pneumatic chambers causes greater colon dilation and compression of the mesentery. The illustrated line graph represents the measured forces at the sampling frequency (10 Hz). The highest value between the two sensors is plotted in the graph. The corresponding boxplot (Fig. 6(c)) illustrates the median, 25th, and 75th percentiles for all three experiments and for the total set of data, with a red cross representing outliers. In all three experiments, the force is higher at the S1 location, near the anatomical curve.

B. Reconstruction Test

A realistic colon phantom has been manufactured to demonstrate a proof of concept of the assistive map reconstruction

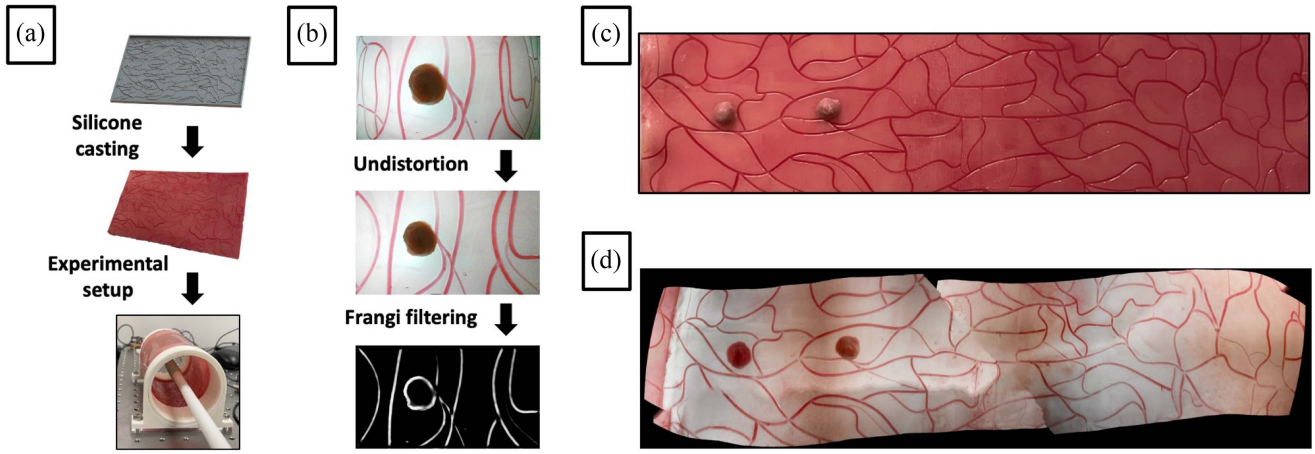

Fig. 7. Colon reconstruction test. (a) The realistic colon phantom is manufactured by casting pigmented silicone on a 3D printed mould. The resulting sheet is then shaped into a cylinder and positioned on two 3D printed supports to establish the experimental setup. In this configuration, tests are conducted in a straight-line simplified scenario using a rigid endoscope mock-up and rigid overtube. (b) An illustrative frame processing process. Each frame collected by the device is undistorted and then processed with Frangi filtering to obtain an intensity map used for image stitching. (c) Top view of the ground truth pattern to be reconstructed. Two silicone polyp phantoms are glued at random positions within the pattern. (d) Reconstruction of the target pattern obtained by stitching together images from two consecutive 360° rotations of the device. Polyps are easily identified in the image and their morphology is maintained. The visible fractures within the panorama result from changes in lighting and variations in boundaries between the registered mosaics, rather than geometric errors, as the vessels are well aligned.

capabilities of the prototype. This phantom has been realised via silicone casting on a flat 3D printed mould with a relief of extruded vessels. The vessel network has been obtained by tracing vessels from three colonoscopy frames extracted from the EndoMapper dataset [8]. The vessel relief is then obtained by extruding circles along the traced curves, with diameters ranging from 0.5 to 1.5 mm. Fig. 7(a) illustrates the moulding and manufacturing processes. Pink EcoFlex 00-30 (Smooth-On Inc., USA) silicone is cast on the mould to obtain a silicone sheet with hollow vessels. Upon curing, vessels are filled by spreading the same silicone, pigmented in dark red. The spreading process is manual, using a spatula, and realises a shiny red hue which improves the photo-realism of the phantom. The silicone phantom is then curved into a cylindrical shape and sealed with silicone glue, and installed on fixed 3D-printed supports, creating the experimental setup.

To demonstrate the conservation of polyp morphology during reconstruction, two polyp phantoms have been manufactured using pink EcoFlex 00-10 (Smooth-On Inc., USA) poured within a soft rubber mould indented with a brush to create an ellipsoid shape about 6x4 mm wide at the base. Prior to using the device, the camera has been calibrated using OpenCV libraries to obtain intrinsic camera parameters using a checkerboard (Fig. 5). The first step of the reconstruction pipeline is the extraction of batches of frames from the camera video. The video is down-sampled from 30 to 5 frames per second, storing keyframes with sufficient overlap. Keyframe batches are saved between two magnetic field readings while moving on the SMS. These frames are first undistorted, then converted to greyscale. Greyscale images are processed using a Frangi filter [18], which is designed to extract intensity maps highlighting vessel-like structures. An example of this processing is illustrated in Fig. 7(b). The intensity map of each frame is inputted to an ORB feature extraction algorithm [19]. High-quality features are matched using OpenCV's implementation of the nearest neighbours algorithm with a distance ratio test [20]. Since processing four batches corresponding to a 360° rotation resulted in slow performance, two batches of frames stored between three magnetic field readings and corresponding to a 180° turn are processed at once. Matched features are used to compute the homography transformation between adjacent frames using a RANSAC-based estimator [21] using an OpenCV implementation. Once the homography transformations are computed, the panoramic view is obtained by stitching each image with respect to the central image in the batch. The 180° panorama is then stitched together with the following 180° one using the same pipeline, starting from greyscale conversion, to create a 360° panoramic map. Once two 360° maps are reconstructed, they are stitched vertically to extend the panorama to obtain a broader reconstruction. A preliminary validation test has been carried, reconstructing a section of a realistic colon phantom, whose top view is illustrated in 7(c). The corresponding panorama, as reconstructed by AID-CMR, is illustrated in Fig. 7(d). This panorama consists of two consecutive 360° panoramas stitched together to form a larger one (corresponding to a full 720° rotation). In this proof of concept, the imaging module has been maneuvered about a straight rigid endoscope by a more manageable 3D printed overtube. The phantom is positioned in a straight configuration and illuminated externally. Further work will be conducted to demonstrate the reconstruction of more complex, curved, and deformable colon phantoms.

IV. Discussion and Conclusion

This letter introduces a prototype of AID-CMR, an add-on colonoscopy device dedicated to the generation of assistive digital maps of the colon. The locomotion and reconstruction capabilities of the system have been tested in-vitro, showing

promising results. The system is currently scaled 1.7:1, and the next steps include the miniaturisation, optimisation and improved integration of the device components with a target outer diameter of 23 mm. First, the employed endoscope shall be smaller (e.g., a pediatric enteroscope). When using such enteroscopes, the use of an overtube may be beneficial to improve the overall stiffness of the scope [22]. Therefore, the AID-CMR overtube will be conceived to help improve the overall maneuverability of the working endoscope, acting as a beneficial integral part of the colonoscopy setup. It will be manufactured using approaches such as multi-material 3D printing, with the objective of obtaining a flexible shaft with high torsional stiffness. Moreover, it will host the water, pneumatic and camera lines to limit cable entanglement and risks associated to the helical motion. The SMS will be miniaturised using different materials for both the core and thread. A customised camera will be realised using a smaller high FoV lens. The pneumatic chambers will be optimised in terms of installation, material and shape. Finally, the current generation of the device will be employed to map more complex colon phantoms, and to perform 3D reconstruction, as a means for estimating missed regions during colonoscopy. To this end, monocular depth estimation methods will be used, in conjunction with kinematic models of the camera motion for pose estimation.

ACKNOWLEDGMENT

The authors express gratitude to Dr. Angelo Damone and Jeref Merlin for their valuable consultancy and support during the characterisation tests of this device.

REFERENCES

[1] H. Sung et al., "Global cancer statistics 2020: Globocan estimates of incidence and mortality worldwide for 36 cancers in 185 countries," *CA: Cancer J. Clinicians*, vol. 71, pp. 209–249, 2021.

[2] G. Ciuti et al., "Frontiers of robotic colonoscopy: A comprehensive review of robotic colonoscopes and technologies," *J. Clin. Med.*, vol. 9, 2020, Art. no. 1648.

[3] S. Zhao et al., "Magnitude, risk factors, and factors associated with adenoma miss rate of tandem colonoscopy: A systematic review and meta-analysis," *Gastroenterol.*, vol. 156, pp. 1661–1674, 2019.

[4] A. M. Leufkens et al., "Factors influencing the miss rate of polyps in a back-to-back colonoscopy study," *Endoscopy*, vol. 44, pp. 470–475, 2012.

[5] D. K. Rex et al., "Quality indicators for colonoscopy," *Amer. J. Gastroenterol.*, vol. 110, pp. 72–90, 2015.

[6] A. Rau et al., "Simcol3D–3D reconstruction during colonoscopy challenge," *Med. Image Anal.*, vol. 96, p. 103195, 2024.

[7] T. L. Bobrow et al., "Colonoscopy 3D video dataset with paired depth from 2D-3D registration," *Med. Image Anal.*, vol. 90, 2023, Art. no. 102956.

[8] P. Azagra et al., "EndoMapper dataset of complete calibrated endoscopy procedures," *Sci. Data*, vol. 10, no. 1, pp. 1–16, 2023.

[9] T. Kudo et al., "New-generation full-spectrum endoscopy versus standard forward-viewing colonoscopy: A multicenter, randomized, tandem colonoscopy trial (J-FUSE study," *Gastrointestinal Endoscopy*, vol. 88, pp. 854–864, 2018.

[10] M. Rubin et al., "Expanding the view of a standard colonoscope with the third eye panoramic^{TM} cap," *World J. Gastroenterol.*, vol. 21, pp. 10683–10687, 2015.

[11] J. Troya et al., "New concept for colonoscopy including side optics and artificial intelligence," *Gastrointestinal Endoscopy*, vol. 95, no. 4, pp. 794–798, 2022.

[12] B. Duan et al., "Colorectal cancer: An overview," *Gastrointestinal Cancers*, pp. 1–12, 2022. [Online]. Available: https://pubmed.ncbi.nlm.nih.gov/36343150/

[13] A. Alazmani et al., "Quantitative assessment of colorectal morphology: Implications for robotic colonoscopy," *Med. Eng. Phys.*, vol. 38, pp. 148–154, 2016.

[14] H. Abidi and M. Cianchetti, "On intrinsic safety of soft robots," *Front. Robot. AI*, vol. 4, 2017. [Online]. Available: https://www.frontiersin.org/journals/robotics-and-ai/articles/10.3389/frobt.2017.00005/full

[15] L. Lindenroth et al., "A fluidic soft robot for needle guidance and motion compensation in intratympanic steroid injections," *IEEE Robot. Automat. Lett.*, vol. 6, no. 2, pp. 871–878, Apr. 2021.

[16] M. Verra et al., "Robotic-assisted colonoscopy platform with a magnetically-actuated soft-tethered capsule," *Cancers*, vol. 12, pp. 1–15, 2020.

[17] M. Finocchiaro et al., "Physical simulator for colonoscopy: A modular design approach and clinical validation," *IEEE Access*, vol. 11, pp. 36945–36960, 2023.

[18] A. F. Frangi et al., "Multiscale vessel enhancement filtering," *Lecture Notes Comput. Sci. Including Subseries Lecture Notes Artif. Intell. Lecture Notes Bioinf.*, vol. 1496, pp. 130–137, 1998.

[19] E. Rublee et al., "ORB: An efficient alternative to SIFT or SURF," in *Proc. IEEE Int. Conf. Comput. Vis.*, 2011, pp. 2564–2571.

[20] D. G. Lowe, "Distinctive image features from scale-invariant keypoints," *Int. J. Comput. Vis.*, vol. 60, pp. 91–110, 2004.

[21] M. A. Fischler and R. C. Bolles, "Random sample consensus," *Commun. ACM*, vol. 24, pp. 381–395, 1981.

[22] T. G. Moreels et al., "Renewed attention for overtube-assisted colonoscopy to prevent incomplete endoscopic examination of the colon," *Dis. Colon Rectum*, vol. 56, pp. 1013–1018, 2013.

Open Access funding provided by 'Scuola Superiore "S.Anna" di Studi Universitari e di Perfezionamento' within the CRUI CARE Agreement